

## Modeling, design and testing of the electrostatic shuffle motor

Niels Tas <sup>a,\*</sup>, Jeroen Wissink <sup>c</sup>, Louis Sander <sup>b</sup>, Theo Lammerink <sup>a</sup>, Miko Elwenspoek <sup>a</sup>

<sup>a</sup> MESA Research Institute, University of Twente, P.O. Box 217, 7500 AE Enschede, Netherlands

<sup>b</sup> Philips Research Laboratory, WA 1-2-10, Prof. Holstlaan 4, 5656 AA Eindhoven, Netherlands

<sup>c</sup> 3T BV, Institutenweg 6, Postbus 3639, 7500 DP Enschede, Netherlands

### Abstract

The shuffle motor is a linear electrostatic stepper motor employing a mechanical transformation to obtain large forces and small steps. A model has been made to calculate the step size and the driving voltage as a function of the load force and the motor geometry. The motor consists of three polysilicon layers and has been fabricated using surface micromachining. Tests show an effective step size of about 85 nm and a produced force of 43  $\mu\text{N}$  at 40 V driving voltage. © 1998 Elsevier Science S.A. All rights reserved.

**Keywords:** Electrostatic motor; Linear motor; Stepper motor; Surface micromachining

### 1. Introduction

Linear motors that apply a walking motion are able to add small steps in order to obtain large translations [1–6]. The possibility to combine a high resolution with a large total stroke makes them attractive for applications like high-density data storage or scanning microscopy. In this paper we discuss the design and realization of a polysilicon surface micromachined linear motor, which is activated by electrostatic forces. Electrostatic micro actuators have the advantage of simple fabrication compared to, for example, piezoelectric and electromagnetic micro actuators. An important disadvantage is the relatively low energy density in electrostatic actuators. This limits the product of force and stroke that can be developed. In the shuffle motor we have maximized the generated force firstly by using a parallel plate configuration and secondly by employing a lever. This way a force of more than 1 mN can be produced in an actuator volume of  $100 \times 200 \times 2 \mu\text{m}^3$ , using a driving voltage of only 30 V. The produced steps are small, typically between 10 and 100 nm, and therefore submicrometer positioning accuracy is easily achieved. In the shuffle motor a cyclic motion is used to produce a large stroke of the actuator, by adding the small single steps. The concept of the shuffle motor was already presented in Ref. [7], however the successful realization was difficult due to the lack of an accurate transducer model and due to stiction problems in the clamp feet of the motor. These problems have been overcome now.

### 2. Principle of operation

Fig. 1 shows the principle of the shuffle cycle. First the front clamp is activated and the actuator plate is deflected

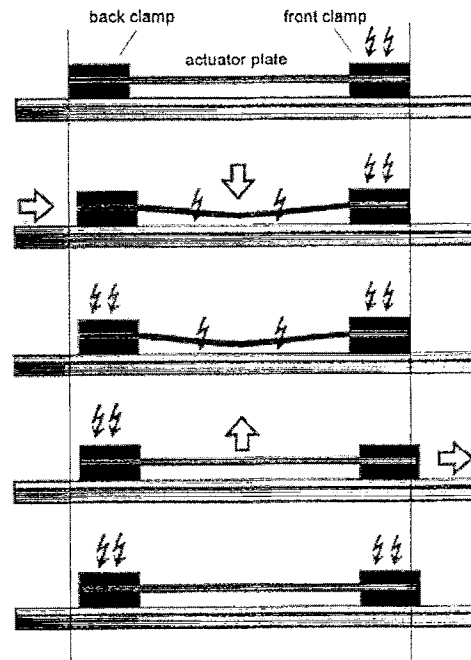


Fig. 1. Principle of operation. First the front clamp is activated and the actuator plate is deflected downward. This causes contraction of the actuator and the back clamp is pulled forward. Next the back clamp is activated, the front clamp and the actuator plate are released. The plate stretches and the front clamp is pushed forward.

\* Corresponding author. E-mail: n.r.tas@el.utwente.nl

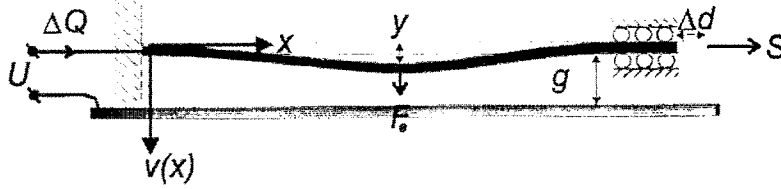


Fig. 2. Ideal physical model of the transducer, where  $x$  is the position along the plate,  $v(x)$  is the deflection of the plate,  $y$  is the center deflection,  $F_e$  is the electrostatic force concentrated in the center,  $g$  is the initial gap size,  $S$  is the tensile load force and  $\Delta d$  is the contraction which produces the step. The transducer converts electrical work  $U \cdot \Delta Q$  into mechanical work  $S \cdot \Delta d$ .

downward. This causes contraction of the actuator and the back clamp is pulled forward. Next the back clamp is activated, the front clamp and the actuator plate are released. The plate stretches and the front clamp is pushed forward. The electrostatic normal force acting on the actuator plate induces a friction force in the feet of about the same magnitude. Due to the built-in mechanical transformation, the developed lateral force can be larger than the friction force and can be high enough to make the feet slide. The deformation of the plate by the electrostatic forces leads to a small but forceful contraction of the plate. A plate length of 200  $\mu\text{m}$  and a center deflection between 0 and 2  $\mu\text{m}$  gives a changing transformation ratio  $i$  from  $\infty$  to 25 [8], where  $i$  is defined as the change of the center deflection  $y$  divided by the change of the lateral contraction  $\Delta d$  (see Fig. 2).

### 3. Model of the transducer

The actuator plate can be considered as an energy buffer with two power ports. It converts the electrical work  $U \cdot \Delta Q$  into mechanical work  $S \cdot \Delta d$  (Fig. 2). An energy model has been made that expresses developed stroke  $\Delta d$  as a function of the tensile load force  $S$  and voltage  $U$  applied between the deflecting plate and the stator electrode.

#### 3.1. Plate stiffness

The deflection of the actuator plate is described by a fourth-order nonlinear differential equation [9]. We have not been able to solve this equation. A solution could be obtained for the case where the electrostatic force is concentrated in the center of the plate, and the case where the electrostatic force is taken uniformly along the plate length. The two shape functions can be used to enclose the solution to the original nonlinear problem, where the electrostatic force distribution depends on the plate deflection. We introduce the model for the central force case here. For the uniformly distributed force case only the results are given (Section 3.4).

The deflection  $v(x)$  of the plate which is under a tensile force  $S$ , due to the central force  $F_e$  (see Fig. 2), is described by the following differential equation:

$$EI \frac{d^4 v(x)}{dx^4} - S \frac{d^2 v(x)}{dx^2} = 0 \quad (1)$$

with boundary conditions  $v(0) = v'(0) = v(l) = 0$  and

$v'''(l) = (1/2) F_e$  and  $EI$  is the bending stiffness. The factor  $1/2$  results from the fact that we solve  $v(x)$  for half of the plate. The solution to Eq. (1) is given by:

$$v(F_e, K, z) = \frac{F_e l^3}{EI} \frac{1 - \cosh(K) - \cosh(Kz) + zK \sinh(K) + \cosh(K(z-1))}{2K^3 \sinh(K)} \quad (2)$$

where  $x$  is the normalized distance using half the plate length  $l$ ,  $z = x/l$  ( $0 < z < 1$ ). The load  $S$  is present in parameter  $K$  which is defined as:

$$K \equiv l \sqrt{\frac{S}{EI}} \quad (3)$$

The parameter  $K$  determines if the transducer is bending dominated or tensile force dominated. The deflection function can be split in an amplitude function  $y(F_e, K)$  equal to the center deflection, and a shape function  $V(K, z)$ . Both amplitude and shape function depend on  $K$ :

$$v(K, z) = y(F_e, K) V(K, z) \quad (4)$$

This way Eq. (2) can be rewritten:

$$y(F_e, K) = \frac{F_e l^3}{24EI} \left\{ \frac{\left(\frac{1}{2}K\right) - \tanh\left(\frac{1}{2}K\right)}{\left(\frac{1}{2}K\right)^3} \right\} \quad (5a)$$

$$V(K, z) = \frac{1 - \cosh(K) - \cosh(Kz) + zK \sinh(K) + \cosh(K(z-1))}{2 - 2 \cosh(K) + K \sinh(K)} \quad (5b)$$

The center deflection  $y$  expressed in Eq. (5a) depends linearly on  $F_e$ . We can therefore derive a stiffness function  $k(K) = F_e/y$ :

$$k(K) = \frac{24EI}{l^3} \left\{ \frac{\left(\frac{1}{2}K\right)^3}{\left(\frac{1}{2}K\right) - \tanh\left(\frac{1}{2}K\right)} \right\} \equiv \frac{24EI}{l^3} G(K) \quad (6)$$

In Eq. (6)  $G(K)$  is the stiffness factor, which is a measure for the stiffening due to the tensile force  $S$ . In Fig. 3a the

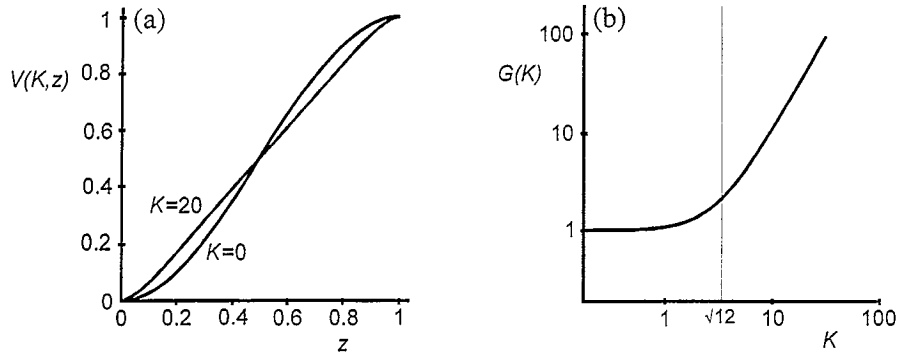


Fig. 3. (a) The shape function  $V(K,z)$  vs.  $z$  for two values of  $K$ . For  $K=0$  the bending stiffness dominates, for  $K=20$  the stiffness due to the tensile force dominates and the plate is pulled straight. (b) The stiffness factor  $G(K)$ . The turnover point  $K=\sqrt{12}$  where stiffening due to the tensile force becomes dominant is indicated.

shape function  $V(K,z)$  is plotted for two values of  $K$ . At  $K=20$  the plate is pulled straight by the tensile load force. Fig. 3b shows the stiffness factor  $G(K)$ . For small  $K$  the effective stiffness is bending dominated and is consistent with the formulas for pure bending [10]:

$$\lim_{K \downarrow 0} k(K) = k_b = \frac{F_e}{y} = 24 \frac{EI}{l^3} \quad (7)$$

For large  $K$  the tensile force acts as an effective stiffness  $F_e/y$  and the normal force  $F_e$  increases linearly with the center deflection  $y$ :

$$\lim_{K \rightarrow \infty} k(K) = k_s = \frac{F_e}{y} = \frac{2EIK^2}{l^3} = \frac{2S}{l} \quad (8)$$

At the turnover point the stiffness ratio is  $k_s/k_b = 1$ . From Eqs. (7) and (8) it follows that this is at  $K^2 = 12$ .

### 3.2. Relation between plate deflection and driving voltage

The plate driven by a constant voltage  $U$  shows pull-in behavior when a certain fraction of the initial gap is closed. The motor will be operated beyond this point of pull-in, therefore it gives a first indication for the driving voltage needed. The full-step size is estimated from the situation where the center of the plate contacts the bottom electrode ( $y = g$ ). Using Eq. (4) and by defining the normalized center deflection  $\alpha = y/g$  we can write for the capacitance:

$$\begin{aligned} C(K,\alpha) &= 2 \int_0^l \frac{\varepsilon w}{g-v(K,x)} dx = 2 \frac{\varepsilon w l}{g} \int_0^1 \frac{1}{1-\alpha V(K,z)} dz \\ &\equiv 2 \frac{\varepsilon w l}{g} C_n(K,\alpha) \equiv C_0 C_n(K,\alpha) \end{aligned} \quad (9)$$

where  $C_n(K,\alpha)$  is the normalized capacitance function,  $C_0$  equals the zero deflection capacitance,  $w$  is the width of the plate and  $\varepsilon$  is the permittivity in the gap. Pull-in behavior of the voltage controlled actuator is studied from the Legendre transformed energy function:

$$\begin{aligned} W'(\alpha,U) &= W(\alpha,U) - QU \\ &= -\frac{1}{2} C_0 C_n(K,\alpha) U^2 + \frac{1}{2} k(K) (\alpha g)^2 \end{aligned} \quad (10)$$

At voltages below the pull-in voltage, a relation between the equilibrium deflection  $\alpha$  and applied voltage  $U$  can be found from setting the first derivative of  $W'(\alpha,K,U)$  equal to zero:

$$U^2 = \frac{2\alpha}{\frac{dC_n}{d\alpha}(K,\alpha)} \frac{k(K) \cdot g^2}{C_0} \quad (11)$$

The equilibrium becomes unstable once the second derivative of  $W'(\alpha,K,U)$  equals zero (turning from positive to negative). Combination with Eq. (11) gives a dimensionless equation for the pull-in deflection. This equation has been solved numerically, yielding a pull-in center deflection increasing from  $\alpha_{pi} = 0.40$  for  $K=0$  to  $\alpha_{pi} = 0.44$  for  $K=\infty$ . Eq. (11) can be rewritten using Eq. (6), the definition of  $C_0$  from Eq. (9), and substitution of  $I = wt^3/12$ :

$$U_{pi} = \pm \sqrt{G(K)} \sqrt{\frac{2\alpha_{pi}}{\frac{dC_n}{d\alpha}(K,\alpha_{pi})} \frac{Et^3 g^3}{\varepsilon l^4}} \quad (12)$$

Where  $t$  is the thickness of the plate. Eq. (12) describes the pull-in voltage as a function of the geometry and the tensile load force  $S$  which is present in the stiffness factor  $G(K)$ . The dimensionless factor  $2\alpha_{pi}/(dC_n(K,\alpha_{pi})/d\alpha)$  increases from 0.75 for  $K=0$  to 0.83 for  $K=\infty$ . For small  $K$  the stiffness factor  $G(K)$  equals 1 and the pull-in voltage is independent of the load force  $S$ :

$$U_{pi} = \pm \sqrt{0.75 \frac{Et^3 g^3}{\varepsilon l^4}} \quad (K \ll \sqrt{12}) \quad (13)$$

For  $K \gg \sqrt{12}$  the pull-in voltage is determined by the load force  $S$  and does not depend on the bending stiffness:

$$U_{pi} = \pm \sqrt{0.83 \frac{Sg^3}{\varepsilon l^2 w}} \quad (K \gg \sqrt{12}) \quad (14)$$

In Fig. 6 the pull-in voltage as a function of the load force  $S$  is plotted for the geometry that is chosen for the realized shuffle motor.

### 3.3. Contraction and transformation ratio

The lateral contraction can be found by calculating the path length along the plate using the deflection function  $v(x)$ . For small slopes  $dv/dx$  the contraction is given by:

$$\Delta d = 2 \int_0^l \sqrt{1 + \left(\frac{dv}{dx}\right)^2} dx - 2l$$

$$\cong \int_0^l \left(\frac{dv}{dx}\right)^2 dx = \frac{y^2}{l} \int_0^1 \left(\frac{dv}{dz}\right)^2 dz \quad (15)$$

where  $y$  is the plate center deflection of the plate and  $z=x/l$  is the normalized position along the plate. The central force shape function  $v$  approximates the triangle shape for large  $K$ . For small  $K$  the curves of the deformed plate are smoother and the path length is slightly larger. Calculating the extremes of the integral in Eq. (15) yields:

$$\lim_{K \downarrow 0} \Delta d = \frac{6}{5} \frac{y^2}{l} \quad (16a)$$

$$\lim_{K \rightarrow \infty} \Delta d = \frac{y^2}{l} \quad (16b)$$

From Eqs. (16a) and (16b) the transformation ratio  $i = \delta y / \delta(\Delta d)$  can be derived:

$$\lim_{K \downarrow 0} i(y) = \frac{5}{6} \frac{l}{2y} \quad (17a)$$

$$\lim_{K \rightarrow \infty} i(y) = \frac{l}{2y} \quad (17b)$$

### 3.4. Uniformly spread electrostatic force model

A similar analysis has been performed for the case where the electrostatic force is spread uniformly along the plate. This results in an expression for the pull-in voltage similar to Eq. (12). The pull-in voltages differ less than 1% for  $K=0$ . For large  $K$  the uniform force shape yields a pull-in voltage that is 5% smaller than for the central force shape. The pull-in deflection is  $y/g=0.40$  for all  $K$ . The contraction for the uniform force case has been calculated using Eq. (15) where the integral yields  $128/105$  for small  $K$  and  $4/3$  for large  $K$ . These slightly larger factors compared to the central force shape are a result of the smoother curves in the plate for the uniform force shape.

The shape functions for the central force model and for the uniformly spread force model enclose the solution to the original nonlinear problem, where the force distribution depends on the deflection. Therefore, we can conclude that

Eq. (12) predicts the pull-in voltage for the nonlinear problem with less than 5% error.

## 4. Design of the shuffle motor

The moving part of the motor consists of two polysilicon layers. A thin layer for the actuator plate, and a thick layer for the frame in which the plate is suspended. The frame consists of a front part and a back part, connected by stretch springs and by the plate. Both the front and the back part contain two clamp feet (Fig. 4). Polysilicon electrodes have been made underneath the feet and the plate, so that the front feet, the back feet and the plate can be activated independently. The electrodes are covered by an insulating silicon nitride layer. The moving part is grounded during operation. The frame is contracted by deflecting the plate downward (Fig. 5), and stretched by means of the stretch springs. The stiffness of the four stretch springs together is about  $12 \mu\text{N}/10 \text{ nm}$ . The whole moving part is supported by two folded springs which serve as a linear guidance with a stiffness of  $1 \mu\text{N}/\mu\text{m}$ . The folded springs are also used to ground the

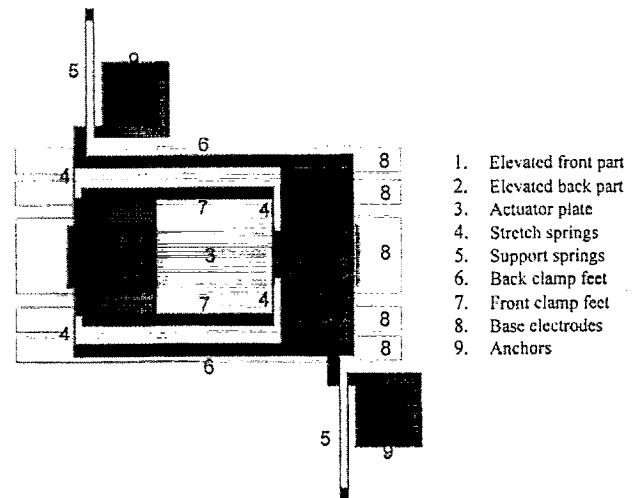


Fig. 4. The frame consists of an elevated part (medium gray) and a lower part (dark gray). The lower part comprises the four clamp feet, resting on the electrodes. The elevated part consists of the folded support springs and the large stiff parts that connect the clamp feet and the actuator plate (light gray). The support springs are anchored at the black squares.

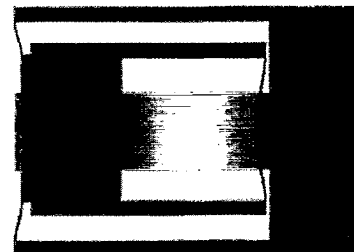


Fig. 5. Deformation of the stretch springs due to contraction of the plate (the step size has been exaggerated). The stretch springs push the two frame parts apart when the plate is released.

moving part. The total size of the moving part excluding the guidance springs is  $500 \times 400 \mu\text{m}^2$ .

#### 4.1. Design of the clamp feet

In the shuffle motor electrically controllable clamp feet are needed, which are continuously in contact with the base. In the first design [7] adhesion forces induced large friction forces, also when the clamps were inactive. In the current design we have been able to reduce the adhesion forces to an acceptable low level by means of anti-sticking bumps that have been made all along the clamp feet. The bumps have a height of 150 nm and are placed with a 10  $\mu\text{m}$  spacing to minimize the bending of the feet due to the high electrostatic pressure. The total area of the two inner clamp feet (the smallest) is  $600 \times 20 \mu\text{m}^2$ . The effective gap between the feet and the base electrode is determined by the size of the bumps and the thickness of the silicon nitride divided by its permittivity. For a clamp voltage of 30 V an electrostatic clamp force of 3 mN is expected. The lifetime of the shuffle motor is probably determined by the wear rate in the clamp feet, particularly in the bumps. The shape and the size of the bumps are not critical, therefore it is expected that the motor will be quite wear resistant.

#### 4.2. Dimensioning of the actuator plate

The plate pull-in voltage given by Eq. (12) is used to choose the actuator dimensions. Fig. 6 shows the pull-in voltage as a function of the load force  $S$  for the chosen dimensions of the actuator: a thickness  $t$  of the plate of 0.5  $\mu\text{m}$ , a width  $w = 100 \mu\text{m}$ , a length  $2l = 200 \mu\text{m}$  and an initial gap size  $g = 2 \mu\text{m}$ . Eqs. (16a) and (16b) give a step size of 40 nm if the center of the plate just contacts the base ( $y = g$ ). This is only an indication for the step size, because the deflection profile after pull-in is not taken into account in the model. Fig. 6 shows that a voltage of only 30 V is enough to overcome a load force of 1 mN. Practically, the maximum load the actuator can pull is limited by the tensile stiffness of the actuator plate. For example in the current design, the tensile strain of the plate under a load of 1 mN is 27 nm, which is significant compared to the single step size. The nature of the load (e.g., friction, dynamic or constant) determines to what extent the limited tensile stiffness will cause loss of step size.

### 5. Fabrication process

On a 3 in. substrate wafer a 1.0  $\mu\text{m}$  low-stress LPCVD silicon nitride layer is grown to insulate the base electrodes from the substrate wafer. Next a 0.5  $\mu\text{m}$  LPVCD polysilicon layer is deposited, doped with boron by solid source indiffusion and patterned using RIE to form the electrodes. A second low-stress LPCVD silicon nitride layer of 0.5  $\mu\text{m}$  is grown to cover the electrodes. In this nitride layer the contact pads and anchor holes are etched using RIE. On top of the

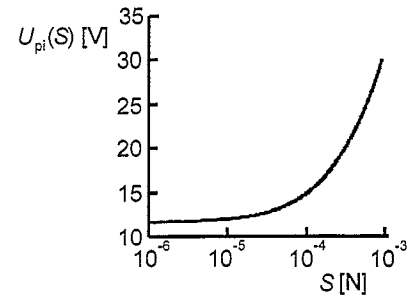


Fig. 6. The pull-in voltage as a function of the load force  $S$ , calculated using Eq. (12). The thickness  $t$  of the plate is 0.5  $\mu\text{m}$ , the width  $w = 100 \mu\text{m}$  and the length  $2l = 200 \mu\text{m}$ . A Young's modulus  $E = 150 \text{ GPa}$  and the permittivity of air are used.

nitride insulation layer the first sacrificial oxide layer (2.4  $\mu\text{m}$ ) is deposited using PECVD to create the gap between the actuator plate and ground electrode. The next layer is 0.5  $\mu\text{m}$  of LPVCD polysilicon doped with boron, to form the actuator plate. After the patterning of the actuator plate (RIE) the first sacrificial layer is patterned (RIE). Only where the elevated parts in the frame are made (Fig. 4) is the oxide kept. Next a 0.5  $\mu\text{m}$  second sacrificial oxide layer is grown, using TEOS instead of PECVD to obtain better step coverage. This layer is used to release the clamp feet. The holes to form the anti-sticking bumps (150 nm deep) and the plate-frame contact holes are etched in HF. Next, a 4.0  $\mu\text{m}$  third LPCVD polysilicon frame layer is deposited and doped. Before patterning this layer, it is covered by a PECVD oxide layer and annealed at 1100°C for 3 h, in order to obtain a uniform distribution of the boron dopant. This is important to avoid a stress gradient in the polysilicon. The thick polysilicon is patterned in RIE using an  $\text{SF}_6/\text{O}_2/\text{CHF}_3$  plasma to form the frame. The last step is removing both sacrificial layers using 50% HF and freeze-drying to avoid sticking of the free hanging structures. Holes have been etched in both the plate and the frame at intervals of 30  $\mu\text{m}$  in order to shorten the sacrificial oxide etch time. In Fig. 7 three cross sections are shown just before and after the sacrificial layer etch. Fig. 8 shows a close up around one of the two inner stretch springs, and an overview of the shuffle motor with the actuator plate deflected downward.

### 6. Test results

#### 6.1. Tests of the plate deflection

The measured zero load pull-in voltage varied between 12 and 13 V. This is reasonably close to the 11 V predicted by the model. Voltages higher than the pull-in voltage resulted in the deflection as shown in Fig. 11. The center part of the actuator plate is pulled flat to the bottom electrode. By increasing the voltage, the flat part increases and the effective step size increases. At 25 V the zero load step size is estimated by 140 nm. Repeated pull-in showed stiction of the actuator plate to the bottom electrode. The stiction is probably induced

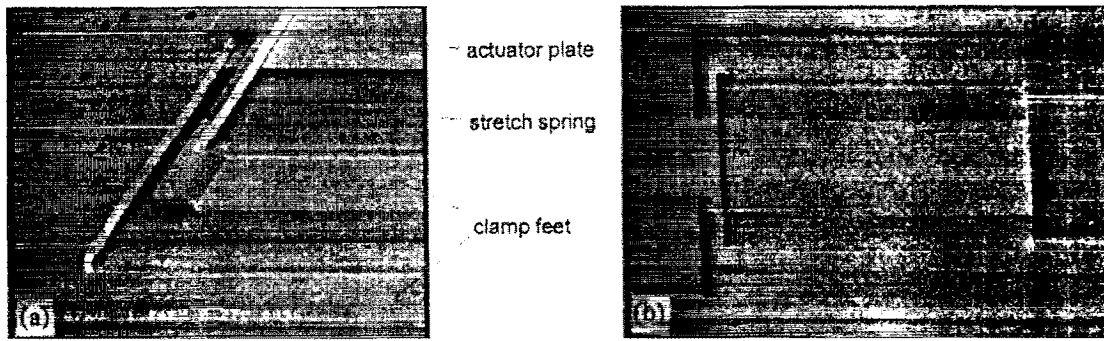


Fig. 7. (a) Close up around one of the two inner stretch springs, showing the different levels in the motor. (b) SEM picture of a motor with the actuator plate deflected downward.

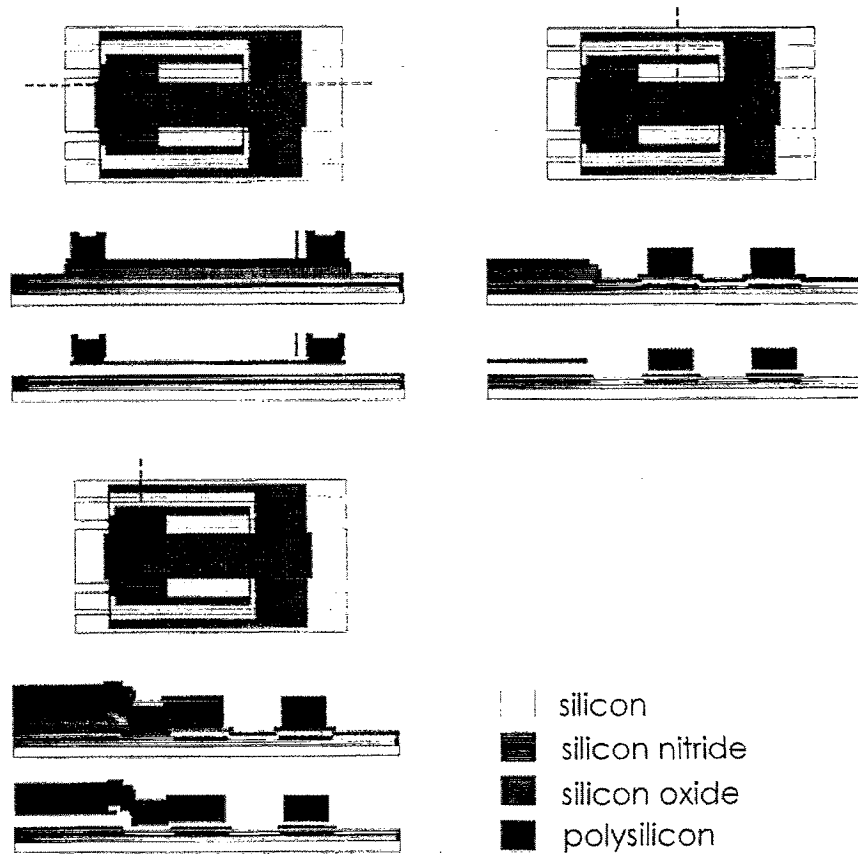


Fig. 8. Cross sections just before and after the sacrificial oxide etching.

by charging of the insulating nitride covering the under electrode. Charge can be transferred from the charged plate to the surface of the silicon nitride when they contact. When the physical contact is broken, some charge may be left on the silicon nitride. The stiction could be strongly reduced by applying a modulated AC voltage (Fig. 9). The plate and the

clamps have been activated with a 25 kHz square wave that changes polarity quickly compared to the mechanical response time of the plate. Therefore, the AC voltage results in the same deflection of the plate as a DC voltage with the same amplitude.

6.2. Force and reach measurement

Motor tests have been done using the control signals shown in Fig. 10. The modulated AC-voltage control has been used for both plate actuation and clamping. The maximum obtained reach was 43 μm (Fig. 11) at a plate actuation voltage (amplitude) of 25 V and a clamp voltage (amplitude) of 40 V and a stepping frequency of 1160 Hz. Based

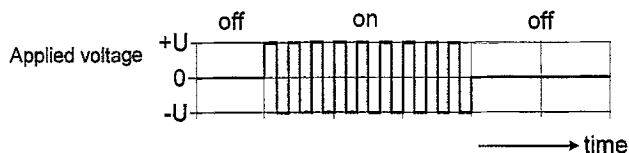


Fig. 9. The modulated AC 2113voltage applied between the plate and the base electrode.

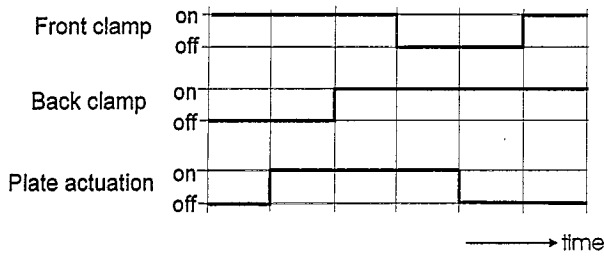


Fig. 10. The control signals for a complete walking cycle. First the front clamp is activated. Next the plate is deflected, and the back clamp is activated. Then the plate is released and the front clamp is activated again. Finally, the back clamp is released and the cycle starts again.

on the stiffness of the support springs, this corresponds with an effective generated force of  $43 \pm 13 \mu\text{N}$ . At 25 V the actuator should be able to produce a force up to 0.6 mN (see Fig. 6). Slip in the clamps is the most probable explanation for the lower measured force. Considerable slip occurs when the AC-driving voltage is used. The clamps are shortly released when the voltage switches from positive to negative. This results in a dynamic equilibrium between walking forward and slipping backward. In order to increase the produced force, we have tried to apply a DC voltage to the clamps in combination with a modulated AC voltage on the actuator plate. This resulted in stiction in the clamps, probably again due to charging of the insulating nitride. A new design of the clamps where the charge induced stiction is diminished is strongly recommended.

### 6.3. Speed measurements

The speed of the motor has been measured as a function of the cycle frequency (Fig. 12). The highest measured speed of the motor is  $100 \pm 10 \mu\text{m/s}$ , at a cycle frequency of 1160 Hz. This frequency was limited by the driving electronics. Higher cycle frequencies should be possible, because the (zero load) resonance frequency of the actuator plate is about 60 kHz. It is expected that the maximum attainable speed is more than 1 mm/s. The measured speeds could be reproduced with a maximum deviation of 25% between three different motors. The slope of the graph is a measure for the effective average step size, which is  $85 \pm 9 \text{ nm}$ . The smaller than

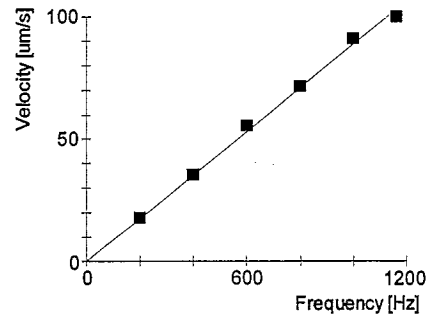


Fig. 12. Measured velocity as a function of the cycle frequency. The inaccuracy in the velocity measurement is smaller than 10%. A voltage amplitude of 25 V is used to drive the plate, and an amplitude of 40 V is used to drive the clamps.

expected effective step size can be explained by the considerable slip in the clamps due to the used AC-driving voltage.

## 7. Discussion and conclusions

This paper shows the feasibility of the use of a mechanical transformation in order to increase both the force and the resolution of an electrostatic linear stepper motor. The key part in the motor is the contracting plate actuator, which is an effective implementation of the mechanical transformation. A detailed energy model of the bending plate transducer has been made, giving the output stroke as a function of the applied voltage and the load force. The model shows that forces as high as 1 mN can be produced with a realistic polysilicon actuator driven at only 30 V. Simple design rules have been extracted that facilitated the design of a stepper motor based on the transducer. Testing of the stepper motor showed stiction due to electrostatic charging of the silicon nitride insulator. The charging could be diminished by a modulated AC-voltage actuation. Stepping motion has been produced at different cycle frequencies. In the measured frequency range (200–1160 Hz), the speed of the motor is proportional to the stepping frequency. An effective average step size of  $85 \pm 9 \text{ nm}$  has been determined from these measurements. A maximum force of  $43 \pm 13 \mu\text{N}$  has been measured at an applied actuator voltage of 25 V and a clamp



Fig. 11. (a) Microscope picture of the inactivated motor, and (b) at maximum measured reach. The maximum measured reach is  $43 \mu\text{m}$ , which corresponds with about 500 steps made. Note that the activated plate is pulled flat against the base electrode.

voltage of 40 V. The generated force is comparable to the force produced by the scratch drive actuators [11]. However, the shuffle motor is operated at slightly lower voltages. The force produced by the shuffle motor is now limited by the effective friction in the clamp feet. Future work should concentrate on the improvement of the clamps in order to have the full benefit of the large force that can be generated by the plate actuator. A new linear guidance, replacing the support springs, has to be developed in order to improve the reach of the motor. Electrical biasing of the moving part will be an important issue when the support springs are omitted.

### Acknowledgements

This research is carried out in cooperation with Philips Research. The authors would like to thank Meint de Boer and Erwin Berenschot for their help with and advice on the processing, and Henri Jansen for helpful discussions about the model and the electrostatic charging. We are thankful to Arie Kooij and Huib van Vossen for making the masks, and Bert Otter for making the SEM photographs.

### References

- [1] T. Akiyama, K. Shono, Controlled stepwise motion in polysilicon microstructures, *J. Microelectromech. Syst.* 2 (3) (1993) 106–110.
- [2] M.P. Koster, A walking piezo motor, *Proc. Actuator '94 Conf.*, Bremen, Germany, June 15–17, 1994, pp. 144–148.
- [3] R. Yeh, E.J.J. Kruglick, K.S.J. Pister, Microelectromechanical components for articulated microrobots, *Proc. 8th Int. Conf. on Solid-State Sensors and Actuators (Transducers '95) and Eurosensors IX*, Vol. 2, 1995, pp. 346–349.
- [4] A. Koga, K. Suzumori, T. Miyagawa, M. Sekimura, Attachment/detachment electrostatic micro actuators for pan-tilt drive of a micro CCD camera, *Proc. IEEE Micro Electro Mechanical Systems '96 Workshop*, San Diego, CA, USA, Feb. 11–15, 1996, pp. 509–514.
- [5] N.R. Tas, A.H. Sonnenberg, A.F.M. Sander, M.C. Elwenspoek, Surface micromachined linear electrostatic stepper motor, *Proc. IEEE Micro Electro Mechanical Systems '97 Workshop*, Nagoya, Japan, Jan. 26–30, 1997, pp. 215–220.
- [6] M. Baltzer, Th. Kraus, E. Obermeier, A linear stepping actuator in surface micromachining technology for low voltages and large displacements, *Proc. 1997 Int. Conf. on Solid-State Sensors and Actuators (Transducers '97)*, Chicago, IL, USA, June 16–19, 1997, Vol. 2, pp. 781–784.
- [7] N.R. Tas, R. Legtenberg, J.W. Berenschot, M.C. Elwenspoek, J.H.J. Fluitman, The electrostatic shuffle motor, *Proc. Micromechanics Europe '95 Workshop*, Copenhagen, Denmark, Sept. 3–5, 1995, pp. 128–131.
- [8] N. Tas, J. Wissink, L. Sander, Th. Lammerink, M. Elwenspoek, The shuffle motor: a high force, high precision linear electrostatic stepper motor, *Proc. 1997 Int. Conf. on Solid-State Sensors and Actuators (Transducers '97)*, Chicago, IL, USA, June 16–19, 1997, Vol. 2, pp. 777–780.
- [9] H.A.C. Tilmans, Micro-mechanical sensors using encapsulated built-in resonant strain gauges, PhD Thesis, University of Twente, 1993, ISBN 90-9005746-3.
- [10] J.M. Gere, S.P. Timoshenko, *Mechanics of Materials*, Chapman & Hall, London, 1991.
- [11] T. Akiyama, H. Fujita, A quantitative analysis of scratch drive actuator using buckling motion, *Proc. IEEE Micro Electro Mechanical Systems '95 Workshop*, Amsterdam, The Netherlands, Jan. 29–Feb. 2, 1995, pp. 310–315.

### Biographies

*Niels Tas* received the MSc degree in electrical engineering from the University of Twente, The Netherlands in 1994. His thesis dealt with the modeling and design of micromachined hydraulic systems. Currently he is working towards a PhD degree at the University of Twente, on the subject of micro-machined linear motors.

*Jeroen Wissink* received the MSc degree in electrical engineering from the University of Twente, The Netherlands in 1997. His thesis dealt with the design and realization of the shuffle motor. Currently he is working at 3T where he is involved in the development of microsensors, microactuators and microsystems.

*Louis Sander* received the MSc degree in physics from the University of Twente, The Netherlands in 1989. He completed a 'technological designer' training in integrated optics in 1991. Since 1992 he has been working at the Philips Research Laboratory in Eindhoven. His current research subject is magnetic shielding of CRT picture tubes.

*Theo Lammerink* received the MSc degree in electrical engineering from the University of Twente, The Netherlands in 1982, and the PhD degree from the same university in 1990. His PhD thesis dealt with the optical actuation and read-out of resonating sensors. Currently he is assistant professor at the Micromechanics Group of the MESA Research Institute, University of Twente. His research interest includes micro-fluidics and micro electromechanical systems with embedded measurement and control.

*Miko Elwenspoek* graduated from the Freie Universitaet Berlin, Germany, in 1977 (physics of liquids). He received the PhD degree in 1983 (nuclear quadrupolar relaxation in liquid alloys) from the same university. From 1983 to 1987 he did research on the kinetics of crystal growth at the University of Nijmegen, The Netherlands. Since 1987 he has been in charge of the Micromechanics Group of the MESA Research Institute, University of Twente, and since 1996 he has been Professor in Transducer Science in the Faculty of Electrical Engineering at the same university. His research interests include device physics, microactuators, microsensors, and etching mechanisms and technology. Dr. Elwenspoek is a member of the MME (Micro Mechanics Europe) Steering Committee and the Micro Electro Mechanical Systems Steering Committee.